

https://dspace.org/

On the constitutive behaviour of the inertial drag with radiative and dissipative heat and chemical reaction for Casson fluid flow over an extending surface through permeable medium

R Baithalu; Titilayo Agbaje; S Panda; S Mishra

https://hdl.handle.net/10539/47315
SCOPUS

Downloaded from a DSpace repository. https://dspace.org/

Partial Differential Equations in Applied Mathematics 14 (2025) 101210

Contents lists available at ScienceDirect

Partial Differential Equations in Applied Mathematics

journal homepage: www.elsevier.com/locate/padiff

On the constitutive behaviour of the inertial drag with radiative and dissipative heat and chemical reaction for Casson fluid flow over an extending surface through permeable medium

Rupa Baithalu [a], Titilayo M Agbaje [b], Subhajit Panda [c], S.R. Mishra [a,*]

[a] Department of Mathematics, Siksha 'O' Anusandhan Deemed to be University, Bhubaneswar, Odisha 751030, India
[b] School of Computer Science and Applied Mathematics, University of the Witwatersrand, Private Bag 3, Braamfontein, Johannesburg 2050, South Africa
[c] Centre for Data Science, Department of Computer Science and Engineering, Siksha 'O' Anusandhan Deemed to be University, Bhubaneswar, Odisha 751030, India

ARTICLE INFO

Keywords:
Casson fluid
Darcy-Forchheimer drag
Thermal radiation
Chemical reaction
Shooting based numerical technique

ABSTRACT

In advanced industrial and biomedical application combined with polymer processing, blood flow analysis, and food processing, the Casson fluid model emerged as a crucial framework for illustrating the transportation of non-Newtonian fluids. The proposed analysis investigates the constitutive behavior of the Darcy-Forchheimer inertial drag considering Casson fluid flow through an extending surface packed with Darcy medium. Also, favorable body forces like radiative and dissipative heat effects and chemical reactions are analyzed to carry out the synergistic role in the thermal and concentration distribution. The suitable assumptions of transformation rules are adopted to transform the governing flow phenomena into dimensionless forms. This leads to the appearance of certain factors involved in these governing equations. Further, coupled nonlinear sets of model problems are handled numerically employing the "spectral Quasi-linearization method". The conformity of the attribute of convergence of the current strategy and the validation with the earlier investigation supported the particular cases. Further, the behaviour of the controlling factors on the flow profiles is depicted graphically. The results reveal the effective interaction of inertial drag and radiant heat on the velocity vis-a-vis temperature distributions. Moreover, the illustration of the enhanced chemical reaction influences the concentration profile with stronger reactions leading to sharper gradients.

1. Introduction

A non-Newtonian fluid model described as the Casson fluid is distinguished by its yield stress behaviour, which means that it only flows when the applied shear stress surpasses a critical threshold. This model is particularly useful in describing biological fluids such as blood and industrial materials like chocolate and honey. In thermal engineering, the study of Casson fluid dynamics under varying conditions, such as magnetohydrodynamic effects or temperature-dependent viscosity, has gained attention due to its applications in medical devices and manufacturing processes. Investigations often focus on its heat and mass transfer properties when subjected to external forces or complex geometries, offering insights for optimizing cooling systems and enhancing energy efficiency. Saleem et al.[1] investigated the behaviour of a Casson tri nanoliquid via a vertically enlarging sheet, considering Thomson and Torian slip constraints and the effects of electromagnetohydrodynamic. This composite nanofluid, referred to as Ag-Cu-TiO_2/Oil, is subjected to gravitational forces influencing free convection. To increase the energy equation's practical relevance, the analysis also considers the influence of a heat release/emission, radiant heat, thermal slip, a porous medium, and Ohmic heating. These considerations lead to a mathematical model comprising PDEs which are simplified to ODEs via an adequate similarity variable. The resulting system of ODEs is solved using the "Runge–Kutta–Fehlberg (RKF-45) method". Saleem et al.[2] reported a comparative analysis of Hiemenz flow in a hybrid Carreau nanofluid, taking viscous dissipation, newtonian heating, and nonlinear effects into account. Lastly, Saleem et al.[3] investigated the Darcy-Forchheimer Casson model numerically, incorporating 2nd-order momentum slip, and gained valuable insights into the complex system's thermal behaviour. Krishna et al.[4] investigate the effect of Newtonian heating on thermal attribute in the MHD transportation of Casson fluid. The standard PDEs are solved by implementing the "Laplace transform method". Presently, graphical

* Corresponding author.
E-mail address: satyaranjan_mshr@yahoo.co.in (S.R. Mishra).

https://doi.org/10.1016/j.padiff.2025.101210
Received 28 December 2024; Received in revised form 15 March 2025; Accepted 23 April 2025
Available online 24 April 2025
2666-8181/© 2025 The Author(s). Published by Elsevier B.V. This is an open access article under the CC BY-NC-ND license (http://creativecommons.org/licenses/by-nc-nd/4.0/).

Nomenclature

x, y, z	coordinate axes(m)
u, v, w	velocity components
q_r	radiative heat flux
Pr	Prandtl number
k_p^*	permeable medium
β	Casson parameter
K_r^*	chemical reaction
Da	Darcy number
Fr	non-inertia drag parameter
Ec	Eckert number
Sc	Schmidt number
Kr	chemical reaction parameter
Nr	radiation parameter
Cf_x, Cf_y	skin friction along x, y direction
Nu_x	Nusselt number
Sh_x	Sherwood number
q_w	heat flux
q_m	mass flux
$\mathrm{Re}_x, \mathrm{Re}_y$	Reynolds number
μ	dynamic viscosity
ρ	density
ρCp	specific heat capacity
T_w	wall temperature
T_∞	ambient temperature
C_w	wall concentration
C_∞	ambient concentration

representations illustrate the velocity, temperature, and species concentration. This study has significant applications in fields such as hydrology and crude oil purification. The Casson fluid model effectively captures the behavior of non-Newtonian fluids. The flow is influenced by periodic plate oscillations, with a uniform transverse magnetization applied perpendicular to the fluid momentum. Mustafa et al.[5] examined a Casson fluid's thermal flow attributes over a moving flat plate influenced by a parallel free stream. Using a "homotopic approach", they derived analytic solutions in series form for the system of nonlinear PDEs. The study by Baithalu et al.[6] deliberates thermo-solutal transportation in Casson fluid transportation over a widening surface under the influence of Ohmic heating and Darcy dissipation packed with pores. Using proper similarity alterations, the equations which govern in their dimensional format are reformed into a non-dimensional framework. Subsequently, the transformed equations are solved through numerical simulation, employing the bvp4c features in MATLAB. UI Haq et al.[7] examined the non-similar solutions for natural convection transport of magneto-Casson fluid over a heated curved surface along Ohmic heating. Non-similar variables are applied to convert the standard equations into dimensionless PDEs. These equations are further simplified into a system of ODEs via the local non similarity method. Manjunatha[8] conducted a theoretical study on trihybridized fluids using H_2O as the host liquid in a stretchy surface configuration with convective constraints. Nazir et al.[9] addressed the rheological features of tangent hyperbolic fluid, enhanced by trihybrid nanofluids, employing a non-Newtonian base fluid. Wahid et al.[10] addressed nanofluid transportation of substantial heat generation over an exponentially stretched, packed with pores. Ali et al.[11] recently explored entropy formation in hybridized fluid flow via a Riga plate under the involvement of strong suction velocity. In another study, Ali et al.[12] analyzed tri-hybrid nanofluid flow over a suddenly moving surface, considering the mutual interaction of Hall current, ion slip, Newtonian heating, porous substances, radiant heat, and chemical species. They utilized a tri-nanoparticle combination ($Cu–TiO_2–Al_2O_3$/WEG) to achieve enhanced heat transfer efficiency. Rehman et al.[13] proposed the flow characteristics of Jeffery-Hamel motion among non-parallel convergent-divergent channels by incorporating thermal relaxations time. The mathematical simulation of the flow problem led to the construction of governing PDEs that incorporate a range of different factors. Again, Baithalu and Mishra[14] proposed the role of magneto-micropolar fluid for the involvement of thermal buoyancy vis-à-vis the impact of radiating heat and chemical species. Also, the focus of the study is the involvement of applied transverse magnetisation, for the variation of the Peclet number influences the flow profiles. Finally, "*Differential Transform Method (DTM)*" an approximate analytical technique is presented for the solution of the flow model. transformed model Pattnaik et al.[15] focused on the 2D circulation of a conducting polar nanofluid within a parallel channel equipped with permeable medium. Additionally, the flow is influenced by various physical factors, including thermal buoyancy, radiative heat, and substantial heat supplier, which enhance the flow profiles. Furthermore, the coupled nonlinear transformuted equations are solved numerically with the interaction of several factors. Hayat et al.[16] examined $MnFe_2O_4$ Casson aqoues solution transportation via a rotating disk, focusing on Buongiorno model, along with radiating energy and entropy generation. Muhammad et al.[17] analyzed two-dimensional nanofluid flow with suspended carbon nanotubes, addressing convective boundary conditions, the Darcy–Forchheimer model, and entropy generation. Alamarashi et al.[18] analyzed a non-Newtonian micropolar time-dependent hybrid nanofluid, with the interaction of thermal radiation over a radially rotating disc. The specialty of the proposed model is due to the simultaneous involvement of Darcy and Forchheimer's assumptions. The impact of magnetization along Joule and Darcy dissipation. Baithalu et al.[19] addressed the transportation of a magneto-polar hybrid nanomaterial on an enlarging surface. Aly et al.[20] reported the convective heat transmission exploiting a hybridized nanomaterial on a surface under the imposition of radiating energy on an elastic sheet. Bellman and Kalaba[21] described quasilinearization to linearize nonlinear problems, while Motsa[22] introduced a spectral local linearization method for improved accuracy in boundary-layer flows. Yanala et al.[23] explored heat and mass transfer in 3D MHD Casson fluid flow, emphasizing radiation and chemical reaction effects, and this study extends such methodologies by integrating novel computational approaches for improved solution efficiency. Furthermore, Rafiq et al.[24] investigated the consequence of viscous dissipation and thermal radiation on micropolar fluid motion induced by cilia with slip conditions, while Mujahid et al.[25] examined magnetized non-Newtonian Casson fluid flow between corrugated curved walls. Additionally, Shahzad et al.[26] conducted a molecular dynamics analysis on the thermal radiatively pressure-driven motion of hybrid nanofluids through a curved pipe, whereas Shahzad et al.[27] explored the rheological behavior of viscous and Casson fluids in a heated curved pipe. Abbas et al.[28] further extended this understanding by analyzing oscillatory movement in an irregular porous channel with slip constraints. Bejawada and Yanala[29] investigated the Soret and Dufour effects in an unsteady MHD flow past an inclined plate, while Reddy et al.[30] explored hydromagnetic radiative stagnation point transportation over a stretching surface. The implication of MHD free convective Casson fluid flow in the presence of Soret, Dufour, and chemical reactions was further evaluated by Kumar et al.[31] Additionally, Shankar Goud et al.[32] presented numerical insights into thermal flow attributes of nanofluids on an inclined revolving disk with chemical reactions, and Bejawada et al.[33] performed a study on radiative electromagnetic nanofluid transportation with viscous dissipation along a vertical plate.

Scientific deficiencies: Investigation on the flow of Casson fluid is not new but limited analysis was presented till date.

- Insufficient studies address the integrating role of inertial drag and radiative heat transfer along with chemical reactions on non-Newtonian fluids such as Casson fluid within a Darcy medium.
- Limited investigations on the interplay between the dissipative heat i.e. the impact of viscous and Darcy dissipation in enhancing the heat transport phenomenon.
- Minimal exploration was carried out for the imposition of chemical reaction on the solutal transport profile of the Casson fluid model.

Targeted study: Based on the importance of unrevealed works for the flow of the Casson model, the following are the main goals of the study.

- To explore the constructive behavior of the inertial drag affecting the fluid momentum and thermal behavior of the Casson fluid flow through an extending surface.
- To explore the mutual impact of radiating energy, Darcy dissipation, and chemical reactions on the heat and solutal transport phenomena.
- To execute a robust numerical technique in handling the coupled nonlinear transport profiles.
- To analyze the significant and effective properties of the factors useful in industrial and biomedical applications.

Original contributions of this research: Motivated by the above-mentioned studies and lack of investigations the originality of the proposed studies is;

- Comprehensive studies of Darcy-Forchheimer drag integrating the impact of thermal radiation into the analysis of Casson fluid.
- Integration of Joule dissipation and chemical reaction for the flow over an extending surface within a permeable medium shows synergetic effects.
- Contribution of advanced numerical method equipped with shooting technique to achieve high accuracy and convergence of the problem.

Key research questions: The proposed analysis brings several questioners those are helpful in investigation the study as well as future prospective.

- How inertial drag due to the Darcy-forchheimer model affect the fluid momentum of Casson fluid flow over an extending surface?
- What are the key features of the thermal radiation and the dissipative heat on the heat transfer phenomenon?
- How chemical reaction influences the solutal profile and mass transfer characteristic over the extending surface?
- Can the numerical methodology ensure the accurate prediction of the behavior of the system in varying conditions?

2. Mathematical formulation

A three dimensional incompressible Casson fluid flow filled with porous along a stretching surface. The sheet is enlarged along the xy-plane and stretching velocities are presented by $u_w = ax$, $v_w = by$ in $x-$ and $y-$ directions, while the fluid is placed along the $z-$ axis. let (u, v, w) denote the velocity component towards (x, y, z)(Fig. 1). The momentum equations account for permeability effects, and nonlinear drag forces in the presence of porosity. The energy equation incorporates radiative heat flux, viscous and Darcy dissipation, reflecting the heat transfer characteristics of the system. Additionally, the mass transport equation considers convective and diffusive effects, including a reaction term influencing species concentration. The boundary conditions specify velocity variations, thermal conditions, and species concentration at the surface, ensuring realistic constraints for the fluid system

The rheological standard equation of a Casson fluid is defined as

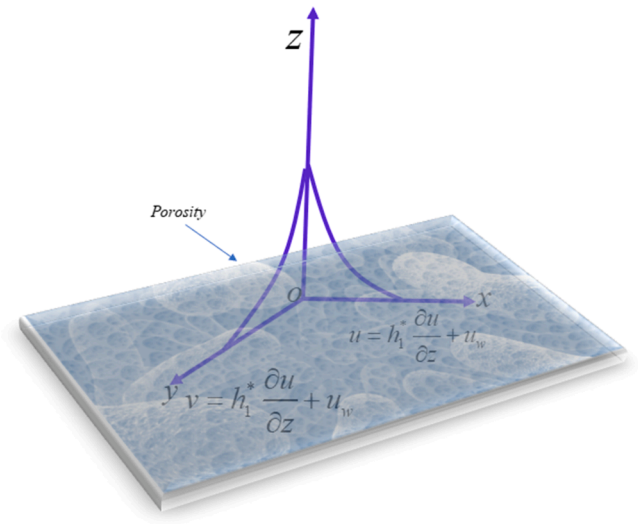


Fig. 1. Flow geometry of the current model.

$$T_{ij} = \left\{ 2\left(\mu_B + \frac{P_z}{\sqrt{2\pi}}\right) e_{ij}, \pi > \pi_c \,\&\, 2\left(\mu_B + \frac{P_z}{\sqrt{2\pi}}\right) e_{ij}, \pi < \pi_c \right\} \tag{2.1}$$

Where $\pi = e_{ij}e_{ij}$with e_{ij} is the $(ij)^{th}$ element of the fluid deformation rate and $p_z = \frac{\mu_B\sqrt{2\pi_c}}{\beta}$ is the yield stress.

The standards equations are expressed as (Yanala et al.[23])

$$u_x + v_y + w_z = 0 \tag{2.2}$$

$$uu_x + vu_y + wu_z = \upsilon\left(1 + \frac{1}{\beta}\right)u_{zz} - \frac{\mu}{\rho k_p^*}u - \frac{C_b}{\sqrt{k_p^*}}u^2, \tag{2.3}$$

$$uv_x + vv_y + wv_z = \upsilon\left(1 + \frac{1}{\beta}\right)v_{zz} - \frac{\mu}{\rho k_p^*}v - \frac{C_b}{\sqrt{k_p^*}}v^2, \tag{2.4}$$

$$uT_x + vT_y + wT_z = \frac{k}{\rho Cp}T_{zz} - \frac{1}{\rho Cp}(q_r)_z + \frac{\mu}{\rho Cp}(u_z)^2 + \frac{\mu}{\rho Cpk_p^*}u^2 \tag{2.5}$$

$$uC_x + vC_y + wC_z = DC_{zz} - K_r^*(C - C_\infty). \tag{2.6}$$

The associated surface constraints are

$$\left.\begin{array}{l} v = v_w(y) = ay, u = u_w(x) = ax, w = 0, C = C_w, T = T_w, \text{ at } z = 0 \\ v \to 0, u \to 0, T \to T_\infty, C \to C_\infty \end{array}\right\} \tag{2.7}$$

$q_r$denoted the radiative heat flux (utilizing the Rosseland estimation) is defined as

$$q_r = -\frac{4\sigma^*}{3k^*}(T^4)_z \tag{2.8}$$

Expanding the term T^4through the truncated Taylor series about T_∞.

$$T^4 = T_\infty^4 + 4T_\infty^3(T - T_\infty) + 6T_\infty^2(T - T_\infty)^2 + \ldots. \tag{2.9}$$

The result of Eq. (2.8) When we exclude the second- and higher-order terms is

$$T^4 = 4T_\infty^3 T - 3T_\infty^4 \tag{2.10}$$

Now replacing Eq. (2.9) in Eq. (2.7) we get

$$q_r = -\frac{16\sigma^* T_\infty^3}{3k^*}T_z \tag{2.11}$$

Implementing (10), Eq. (5) can be expressed as

$$uT_x + vT_y + wT_z = \frac{k}{\rho Cp}T_{zz} + \frac{1}{\rho Cp}\left(\frac{16T_\infty^3\sigma^*}{3k^*}T_{zz}\right) + \frac{\mu}{\rho Cp}(u_y)^2 + \frac{\mu}{\rho Cpk_p^*}u^2 \tag{2.12}$$

Introducing the following similarity functions are

$$\left.\begin{aligned} u = axf'(\eta), v = ayg'(\eta), w = -\sqrt{av}\{f(\eta)+g(\eta)\},\\ \eta = \sqrt{\frac{a}{v}}, \theta = \frac{T-T_\infty}{T_w-T_\infty}, \phi = \frac{C-C_\infty}{C_w-C_\infty}\end{aligned}\right\}. \tag{2.13}$$

Applying the above-mentioned similarity functions in the main standard equations take the form of

$$\left(1+\frac{1}{\beta}\right)f''' + ff'' + gf'' - f'^2 - Daf' - Frf'^2 = 0 \tag{2.14}$$

$$\left(1+\frac{1}{\beta}\right)g''' + fg'' + gg'' - g'^2 - Dag' - Frg'^2 = 0 \tag{2.15}$$

$$(1+Nr)\theta'' + \Pr f\theta' + \Pr g\theta' + \Pr Ecf''^2 + \Pr EcDaf'^2 = 0 \tag{2.16}$$

$$\phi'' + Scf\phi' + Sc\phi' g - KrSc\phi = 0 \tag{2.17}$$

the modified surface constraints are

$$\left.\begin{aligned} f(0)=0, g(0)=0, f'(0)=1, g'(0)=1, \theta(0)=1, \phi(0)=1\\ f'(\infty)\to 0, g'(\infty)\to 0, \theta(\infty)\to 0, \phi(\infty)\to 0.\end{aligned}\right\} \tag{2.18}$$

concerning the relevant physical characteristics, where

$$M = \frac{\sigma B_0^2}{\rho a}, \Pr = \frac{\mu Cp}{k}, Da = \frac{\mu}{k_p^* a}$$
$$Sc = \frac{v}{D_M}, Nr = \frac{16\sigma^* T_\infty^3}{3kk^*}, Kr = \frac{Kr^*}{a}, Ec = \frac{u_w^2}{Cp(T_w - T_\infty)} \tag{2.19}$$

The important physical aspects are presented as

$$Cf_x = \frac{\tau_{wx}}{\rho u_w^2} \Rightarrow \left(\sqrt{\mathrm{Re}_x}\right)Cf_x = \left(1+\frac{1}{\beta}\right)f''(0) \tag{2.20}$$

$$Cf_y = \frac{\tau_{wy}}{\rho u_w^2} \Rightarrow \left(\sqrt{\mathrm{Re}_y}\right)Cf_y = \left(1+\frac{1}{\beta}\right)g''(0) \tag{2.21}$$

$$Nu_x = \frac{xq_w}{k(T_w - T_\infty)} where q_w = -k\left(\frac{\partial T}{\partial z}\right)_{z=0} + q_r|_{z=0} \Rightarrow (\mathrm{Re}_x)^{-\frac{1}{2}}Nu_x = -(1+Nr)\theta'(0) \tag{2.22}$$

$$Sh_x = \frac{xq_w}{D(C_w - C_\infty)} where q_m = -D\left(\frac{\partial C}{\partial z}\right)_{z=0} \Rightarrow (\mathrm{Re}_x)^{-\frac{1}{2}}Sh_x = -\phi'(0) \tag{2.23}$$

Where $\mathrm{Re}_x = \frac{u_w(x)x}{v}$ & $\mathrm{Re}_y = \frac{v_w(y)y}{v}$ are the local Reynolds number.

Method of Solution

To solve the system of nonlinear ODEs described by Eqs. (2.14)–(2.17) along with the boundary conditions in (2.18), we utilized the "Spectral Quasi-linearization Method (SQLM)" and implemented the corresponding algorithm in MATLAB. This method incorporates the "Quasi-linearization approach", inspired by the "Newton-Raphson method", to linearize the nonlinear equations. Originally proposed by Bellman and Kalaba[21] in 1965, the "Quasi-linearization Method (QLM)" achieves linearization by expanding the nonlinear terms in the governing equations using a Taylor series. This expansion assumes that the difference between the values of the unknown function in the current iteration $m+1$ and the previous iteration m is small. For a comprehensive explanation of this approach, refer to the work of Motsa.[22] After linearizing the system, the "Chebyshev spectral collocation method" is employed to solve it, enhancing both computational efficiency and accuracy. The iterative process converges rapidly, providing precise results. By applying the quasi-linearization technique to Eqs. (2.13)–(2.15), the system is transformed into a new set of equations as follows:

$$\alpha_{0,m}f'''_{m+1} + \alpha_{1,m}f''_{m+1} + \alpha_{2,m}f'_{m+1} + \alpha_{3,m}f_{m+1} + \alpha_{4,m}g_{m+1} = Y_f, \tag{2.24}$$

$$\delta_{0,m}g'''_{m+1} + \delta_{1,m}g''_{m+1} + \delta_{2,m}g'_{m+1} + \delta_{3,m}g_{m+1} + \delta_{4,m}f_{m+1} = Y_g, \tag{2.25}$$

$$\gamma_{0,m}\theta''_{m+1} + \gamma_{1,m}\theta'_{m+1} + \gamma_{2,m}f''_{m+1} + \gamma_{3,m}f'_{m+1} + \gamma_{4,m}f_{m+1} + \gamma_{5,m}g_{m+1} = Y_\theta, \tag{2.26}$$

$$\Lambda_{0,m}\phi''_{m+1} + \Lambda_{1,m}\phi'_{m+1} + \Lambda_{2,m}\phi_{m+1} + \Lambda_{3,m}f_{m+1} + \Lambda_{4,m}g_{m+1} = Y_\phi, \tag{2.27}$$

The variable coefficients $\alpha_{k,m}$, $\delta_{k,m}$, $\gamma_{k,m}$, and $\Lambda_{k,m}$, ($fork = 1, 2, 3, \ldots$) in Eqs. (2.24)–(2.27) are expressed as:

$$\begin{aligned}\alpha_{0,m} &= \left(1+\frac{1}{\beta}\right), \quad \alpha_{1,m} = f_m + g_m, \quad \alpha_{2,m}\\ &= -2f'_m - Da - 2Frf'_m, \quad \alpha_{3,m} = f''_m, \quad \alpha_{4,m} = f''_m,\end{aligned}$$

$$\begin{aligned}\delta_{0,m} &= \left(1+\frac{1}{\beta}\right), \quad \delta_{1,m} = f_m + g_m, \quad a_{2,m}\\ &= -2g'_m - Da - 2Frg'_m, \quad a_{3,m} = g''_m, \; a_{4,m} = g''_m\end{aligned}$$

$$\begin{aligned}\gamma_{0,m} &= (1+Nr), \quad \gamma_{1,m} = Prf_m + Prg_m, \quad \gamma_{2,m} = 2f''_m PrEc, \quad \gamma_{3,m}\\ &= 2f'_m PrEcDa, \gamma_{4,m} = Pr\theta'_m, \; \gamma_{5,m} = Pr\theta'_m\end{aligned}$$

$$\begin{aligned}\Lambda_{0,m} &= 1, \quad \Lambda_{1,m} = Scf_m + Scg_m, \quad \Lambda_{2,m} = -KrSc, \quad \Lambda_{3,m}\\ &= Sc\phi'_m, \quad \Lambda_{4,m} = Sc\phi'_m,\end{aligned} \tag{2.28}$$

The right-hand side of Eqs. (2.24)–(2.27) are given as:

$$Y_f = f_m f''_m + g_m f''_m - f'^2_m - Frf'^2_m,$$

$$Y_g = f_m g''_m + g_m g''_m - g'^2_m - Frg'^2_m,$$

$$Y_\theta = Prf_m\theta'_m + Prg_m\theta'_m + PrEcf''^2_m + PrEcDaf'^2_m,$$

$$Y_\phi = Scf_m\phi'_m + Scg_m\phi'_m. \tag{2.29}$$

Using appropriate initial guesses, the iterative schemes in Eqs. (2.24)–(2.27) are solved repeatedly to determine f_{m+1}, g_{m+1}, θ_{m+1}, and ϕ_{m+1}. The obtained initial guesses to initiate the iterative schemes are:

$$f_0(\eta) = 1 - e^{-\eta}, \quad g_0(\eta) = 1 - e^{-\eta}, \quad \theta_0(\eta) = e^{-\eta}, \quad \phi_0(\eta) = e^{-\eta}. \tag{2.30}$$

To compute numerical solutions for Eqs. (2.24)–(2.27), the Chebyshev spectral collocation method is applied for discretization. This technique operates within the interval $[-1, 1]$, where calculations are performed. Because the problem's original domain is semi-infinite, domain truncation is necessary before employing the spectral method. The semi-infinite domain is approximated by a finite domain$[0, L]$, with L chosen sufficiently large to capture the behavior of the solution at infinity. To facilitate this, the transformation $\eta = L(\zeta + 1)/2$is used, which maps the truncated domain $[0, L]$ onto the interval$[-1, 1]$. This transformation enables the application of the spectral method on a finite domain while preserving the solution's accuracy.

Additionally, a differentiation matrix $D$is employed to approximate

the derivatives of the unknown functions $f(\eta)$, $g(\eta)$, $\theta(\eta)$and $\phi(\eta)$at the specified collocation points. This approximation is achieved by performing a matrix-vector product, which can be expressed as:

$$\left.\begin{aligned} \frac{df}{d\eta} &= \sum_{s=0}^{N_x} D_{st} f(\zeta_t) = DF, \quad t = 0,1,2,\ldots N_x, & \frac{d\theta}{d\eta} &= \sum_{s=0}^{N_x} D_{st}\theta(\zeta_t) = D\Theta, \quad t = 0,1,2,\ldots N_x \\ \frac{dg}{d\eta} &= \sum_{s=0}^{N_x} D_{st} g(\zeta_t) = DG, \quad t = 0,1,2,\ldots N_x, & \frac{d\phi}{d\eta} &= \sum_{s=0}^{N_x} D_{st}\phi(\zeta_t) = D\Phi, \quad t = 0,1,2,\ldots N_x. \end{aligned}\right\} \tag{2.31}$$

In the above, N_x is the number of collocation points, $\boldsymbol{D} = 2D/L$, and

$F = [f(\zeta_0),\ f(\zeta_1),\ldots,f(\zeta_{N_x})]^T, \Theta = [\theta(\zeta_0),\ \theta(\zeta_1),\ldots,\theta(\zeta_{N_x})]^T$
$G = [g(\zeta_0),\ g(\zeta_1),\ldots,g(\zeta_{N_x})]^T, \Phi = [\phi(\zeta_0),\ \phi(\zeta_1),\ldots,\phi(\zeta_{N_x})]^T$

The SQLM method for Eqs. (2.24) to (2.27) can be compactly represented in matrix form as:

$$\begin{bmatrix} A_{11} & A_{12} & A_{13} & A_{14} \\ A_{21} & A_{22} & A_{23} & A_{24} \\ A_{31} & A_{32} & A_{33} & A_{34} \\ A_{41} & A_{42} & A_{43} & A_{44} \end{bmatrix} \begin{bmatrix} f_{m+1} \\ g_{m+1} \\ \theta_{m+1} \\ \phi_{m+1} \end{bmatrix} = \begin{bmatrix} \mathrm{Y}_f \\ \mathrm{Y}_g \\ \mathrm{Y}_\theta \\ \mathrm{Y}_\phi \end{bmatrix}. \tag{32}$$

In the above,

$$A_{11} = [\alpha_{0,m}]\boldsymbol{D}^3 + diag[\alpha_{1,m}]\boldsymbol{D}^2 + diag[\alpha_{2,m}]\boldsymbol{D} + diag[\alpha_{3,m}]\boldsymbol{I}, A_{12} = diag[\alpha_{4,m}]\boldsymbol{I}, A_{13} = 0, A_{14} = 0$$

$$A_{21} = diag[\delta_{4,m}]\boldsymbol{I}, A_{22} = [\delta_{0,m}]\boldsymbol{D}^3 + diag[\delta_{1,m}]\boldsymbol{D}^2 + diag[\delta_{2,m}]\boldsymbol{D} + diag[\delta_{3,m}]\boldsymbol{I}, A_{23} = 0, A_{24} = 0,$$

$$A_{31} = diag[\gamma_{2,m}]\boldsymbol{D}^2 + diag[\gamma_{3,m}]\boldsymbol{D} + diag[\gamma_{4,m}]\boldsymbol{I}, A_{32} = diag[\gamma_{5,m}]\boldsymbol{I}, A_{33} = [\gamma_{0,m}]\boldsymbol{D}^2 + diag[\gamma_{1,m}]\boldsymbol{D}, A_{34} = 0,$$

$$A_{41} = diag[\Lambda_{3,m}]\boldsymbol{I},\ A_{42} = diag[\Lambda_{4,m}]\boldsymbol{I},\ A_{34} = 0,\ A_{44} = [\Lambda_{0,m}]\boldsymbol{D}^2 + diag[\Lambda_{1,m}]\boldsymbol{D} + diag[\Lambda_{2,m}]\boldsymbol{I}$$

In the above representation, the symbol *"diag"* represents a diagonal matrix with dimensions $(N_x+1)\times(N_x+1)$, *"**I**"* denotes an identity matrix of size $(N_x+1)\times(N_x+1)$, 0 represents $(N_x+1)\times(N_x+1)$, zero matrix and *"**D**"* signifies differentiation with respect to η.

Table 1
Comparison of $-\left(1+\frac{1}{\beta}\right)f''(0)$,with previously published work of Yanala et al.,[23] for different values of *M*, *K* and β when $Nr = c = Kr = Sc = 0.5$, and $Pr = 0.71$.

M	*K*	β	Yanala et al.[23]	Present Study
0.50	0.50	1.00	1.92434	1.92434448
0.70	0.50	1.00	2.04332	2.04331888
0.90	0.50	1.00	2.19271	2.19271403
1.20	0.50	1.00	2.46175	2.46175285
0.50	0.80	1.00	2.07209	2.07209030
0.50	1.20	1.00	2.25515	2.25515183
0.50	1.60	1.00	2.42508	2.42507961
0.50	0.50	1.20	1.84136	1.84136044
0.50	0.50	1.40	1.77992	1.77992486
0.50	0.50	1.60	1.73253	1.73252499

Table 2
Comparison of $-\theta'(0)$, with previously published work of Yanala et al.,[23] for different values of *Pr*, and *Nr* when$K = M = c = Kr = Sc = 0.5$, and $\beta = 1$.

Pr	*Nr*	Yanala et al.[23]	Present Study
0.71	0.50	0.457552	0.45755206
0.71	1.00	0.403105	0.40310529
0.71	1.50	0.371275	0.37127493
0.71	2.00	0.350116	0.35011624
1.00	0.50	0.545714	0.54571409
1.38	0.50	0.657216	0.65721638
4.00	0.50	1.25038	1.25038138

3. Results and discussions

In this section, the numerical results using the Spectral Quasi-Linearization Method (SQLM), implemented through MATLAB code is analyzed for the problem of magnetised 3D viscous Casson fluid transportation through an expanding surface. This numerical approach effectively solves the governing equations for velocity, temperature, concentration, and motile microorganism distributions. To verify the accurateness and reliability of our results, we compared them with previously published data, as shown in Tables 1, 2, 3 and found excellent agreement with the referenced works. To demonstrate the convergence of the SQLM, we evaluated the solution errors using infinity norms,

Table 3
Comparison of$-\phi'(0)$, with previously published work of Yanala et al.,[23] for different values of *Kr*, and *Sc* when$K = M = c = Nr = 0.5$, $Pr = 0.71$, and $\beta = 1$.

Kr	*Sc*	Yanala et al.[23]	Present Study
0.50	0.22	0.480203	0.48020335
1.00	0.22	0.579555	0.57955504
1.50	0.22	0.666537	0.66653741
2.00	0.22	0.744429	0.74442921
0.50	0.78	0.918652	0.91865230
0.50	1.25	1.192140	1.19214026
0.50	1.60	1.364910	1.36491023

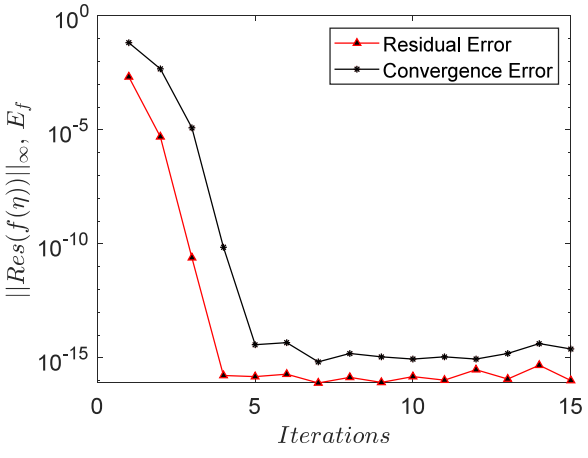


Fig. 2. Solution and residual errors for $f(\eta)$.

which measure the differences in function values between successive iterations, defined as follows:

$$E_f = \max_{0\le p\le N_x} f_{m+1,p} - f_{m,p}{}_\infty, \quad E_\theta = \max_{0\le p\le N_x} \theta_{m+1,p} - \theta_{m,p}{}_\infty,$$

$$E_g = \max_{0\le p\le N_x} \|g_{m+1,p} - g_{m,p}\|_\infty, E_\phi = \max_{0\le p\le N_x} \phi_{m+1,p} - \phi_{m,p}{}_\infty$$

To further confirm the accuracy of the SQLM, we compute the infinity norm of the residual error for each function. This involves substituting the approximate solutions into the governing differential Eqs. (2.8) through (2.11). The respective norms are defined as follows:

$$Res\ (f)_\infty = \|\left(1+\frac{1}{\beta}\right) f_m''' + f_m f_m'' + g_m f_m'' - f_m'^2 - Da f_m' - Frf_m'^2\|_\infty,$$

$$Res\ (g)_\infty = \|\left(1+\frac{1}{\beta}\right) g_m''' + f_m g_m'' + g_m g_m'' - g_m'^2 - Da g_m' - Frg_m'^2\|_\infty,$$

$$Res\ (\theta)_\infty = \|(1+Nr)\theta_m'' + Prf_m\theta_m' + Prg_m\theta_m + PrEcf_m''^2 + PrEcDaf_m'^2\|_\infty,$$

$$Res\ (\phi)_\infty = \|\phi_m'' + Scf_m\phi_m' + Scg_m\phi_m' - KrSc\phi_m\|_\infty,$$

Figs. 2–5 offer a clear illustration of how both convergence and residual errors decrease as the number of iterations increases, effectively showcasing the outstanding accuracy and efficiency of the Spectral Quasi-linearization Method (SQLM). These figures highlight the swift reduction in errors, demonstrating that SQLM quickly converges to an accurate solution with just a few iterations. Specifically, both residual and convergence errors drop significantly after approximately 6 to 7 iterations, suggesting that SQLM not only provides highly precise solutions but also converges rapidly, making it a powerful tool for solving nonlinear systems. The rapid error reduction indicates that the method refines the approximate solutions efficiently with each iteration, achieving high precision without demanding extensive computational resources.

Moreover, the figures emphasize the method's effectiveness in minimizing errors and ensuring overall stability. The residual error, which reflects the discrepancy between the numerical and exact solutions, decreases quickly, indicating the method's strong ability to approximate the true solution. Likewise, the convergence error, which measures the difference between consecutive iterations, approaches zero after just a few iterations, confirming that the solution has stabilized and that further iterations result in only minor changes.

Parametric range

The momentum, energy, and concentration distribution of the Casson fluid over an expanding surface packed with Darcy medium are obtained for the occurrence of several factors involved in these profiles.

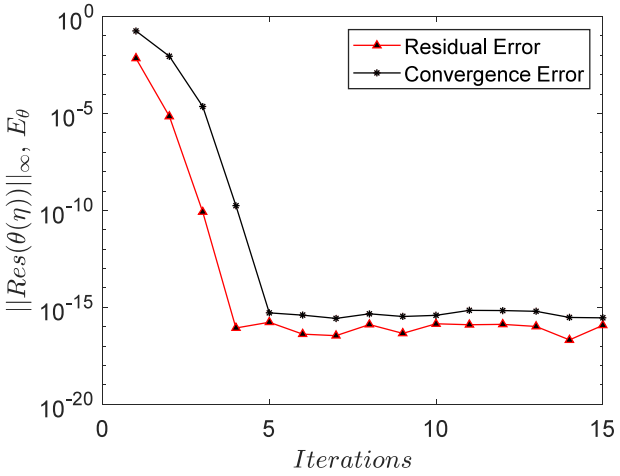


Fig. 4. Solution and residual errors for θ(η).

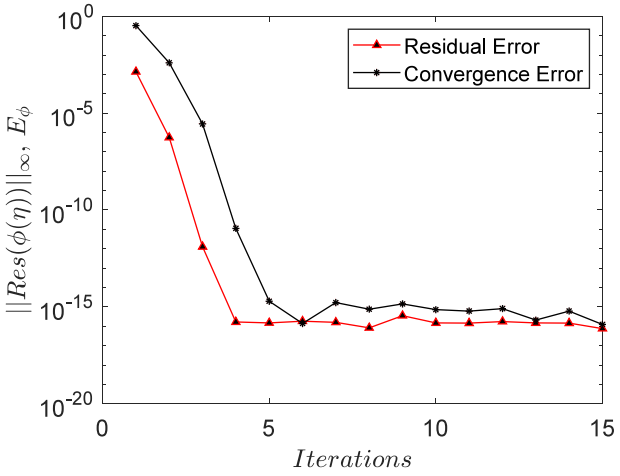


Fig. 5. Solution and residual errors for ϕ(η).

However, the physical properties of these factors on the profiles are obtained for the consideration of their numerical values within certain ranges. The Darcy number quantifies the permeability of the porous medium is chosen within the range of $0.5 \le Da \le 3$whereas the non-Newtonian Casson parameter representing the behavior of the non-

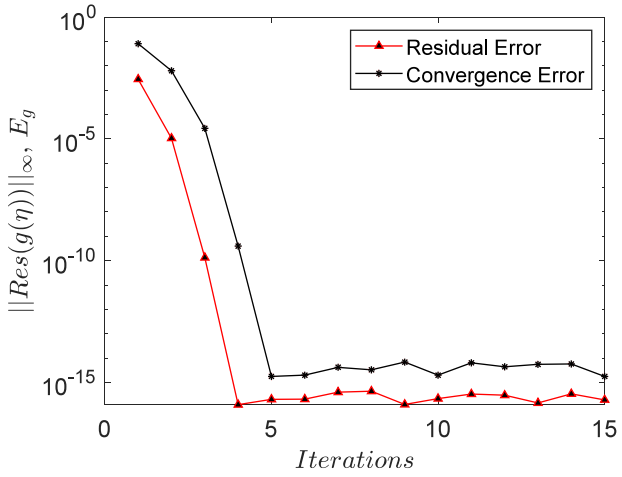


Fig. 3. Solution and residual errors for $g(\eta)$.

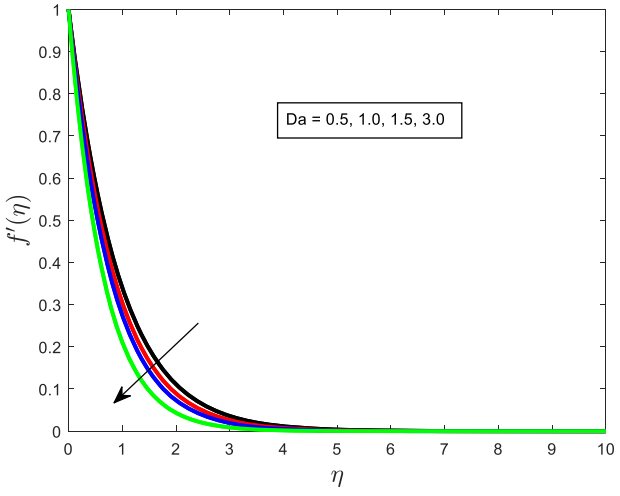


Fig. 6. Change in Da on $f'(\eta)$.

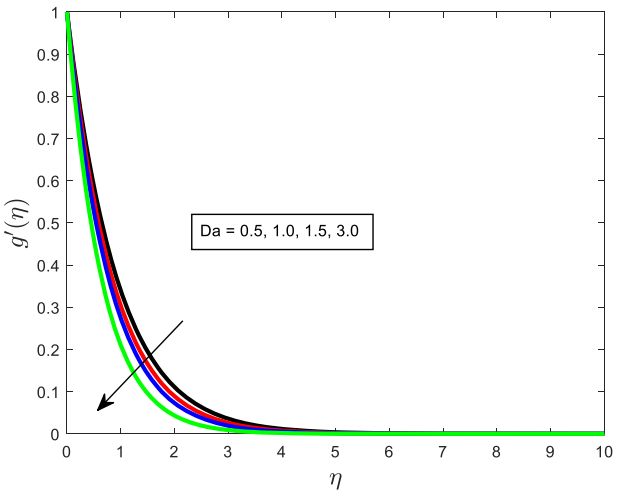


Fig. 7. Change in *Da* on $g'(\eta)$.

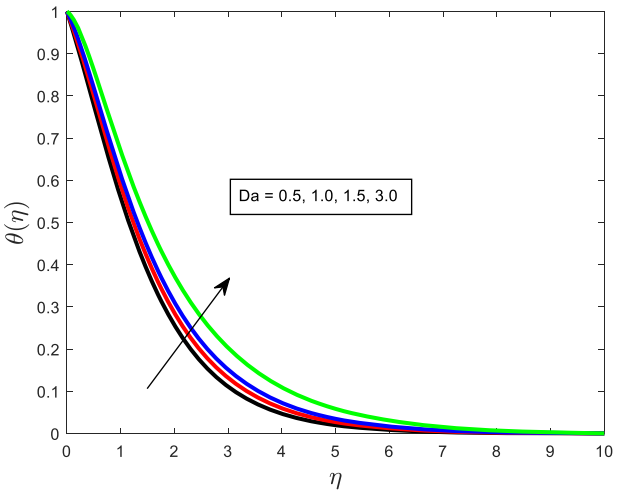


Fig. 8. Change in *Da* on $\theta(\eta)$.

Newtonian fluid on the profiles by considering the numerical range as$0.5 \leq \beta \leq 3$. The Forchheimer inertial drag *Fr* accounts for inertial effects in the porous medium which is presented within the range$0.5 \leq Fr \leq 6$. The behavior of aforesaid factors is depicted on the momentum, and energy distributions. The Eckert number measures the conversion of kinetic energy to thermal energy which is considered as $0.1 \leq Ec \leq 5$and the thermal radiation Nr representing the radiative heat transfer in the system is illustrated as $0.5 \leq Nr \leq 2$.The entire energy system is affected by the Prandtl number which is projected by considering the numerical values as $0.71 \leq Pr \leq 3$.The chemical reaction parameter *Kr* quantifies the rate of chemical reaction in the concentration distribution within the range of $0.5 \leq Kr \leq 2$and finally the Schmidt number *Sc* on the concentration profile is depicted as $0.22 \leq Sc \leq 2$.

Parametric analysis

The physical behaviour of the above-mentioned factors presented through graphs are analysed and described in this proposed section. In particular, Figs. 6–8 depicts the pivotal role of the Darcy number on the flow and heat transfer behavior within the porous medium. The non-zero variation of the factor represents the impact of *Da* on the Casson fluid velocity and temperature distribution. In particular, Fig. 6 demonstrates the characteristic of *Da* on the axial velocity distribution. A low Darcy number signifies high permeability indicates lower resistance of the porous medium which enhances the axial fluid velocity. The more pronounced result is presented for the low resistivity of the permeable medium. Further, with increasing *Da* the permeability decreases which causes enhanced resistivity due to the permeability of the porous medium. This ensures the retardation of the profile and consequently the bounding surface thickness retards significantly. The transverse momentum is also affected by the behavior of the factor *Da* within the proposed range which is depicted in Fig. 7. The lower *Da*, the velocity distribution also exhibits maximum strength within the domain and the effect is due to the lower resistivity impact. Further, with increasing *Da* the transverse flow is minimal, constrained by the inability of the fluid to move freely within the layers. Therefore, the enhanced *Da* decelerates the transverse momentum within the entire domain and the behavior is asymptotic throughout. The illustration of the factor *Da* on the fluid temperature is shown in Fig. 8. The lower *Da* facilitates higher permeability that depends upon the mathematical expression of the Darcy number which performs low resistance. This contributes a low thermal enhancement within the system. However, higher *Da* shows low permeability and reduces the frictional drag as the fluid encounters less resistance. The axial transport of heat becomes more effective resulting a significant increase in the fluid temperature. The augmentation in the fluid temperature distribution is presented with the increase of Darcy number. Particularly, the yield stress characteristic of the Casson fluid dominates with high *Da* further suppressing both axial and transverse velocity. The reduced resistance allows Casson fluid to exhibit its non-Newtonian shear thinning behavior amplifying the velocity profile and enhancing the convective heat transfer.

Applications: The utility of the porous matrix in the fluid flow phenomena has a significant role in various real-world applications. Particularly, in geothermal systems the permeability of the medium influences the efficiency of heat extraction from the reservoirs. Moreover, high permeability allows geothermal fluid water to flow easily through rock formations, enhancing heat transfer rates and making energy extraction more efficiently. Also, permeability is a critical parameter in oil recovery processes.

The illustration of the non-Newtonian Casson fluid parameter affecting the axial and transverse velocity distribution is presented through Figs. 9, 10. For the smaller Casson fluid parameter, $\beta = 0.5$, the Casson fluid behaves more likely a highly shear thinning non-Newtonian fluid. The velocity gradient near the boundaries is steeper indicating a thinner boundary layer. Further, at higher βthe fluid approaches Newtonian behavior and the axial velocity is more uniformly distributed within the flow domain and this causes a smaller velocity gradient close to the boundaries. The transverse velocity is typically affected by the secondary velocity and the behavior is influence by the quantity β. Transverse velocity exhibits more pronounced variation due to higher non-Newtonian effects and shown for the lower β. the enhanced shear

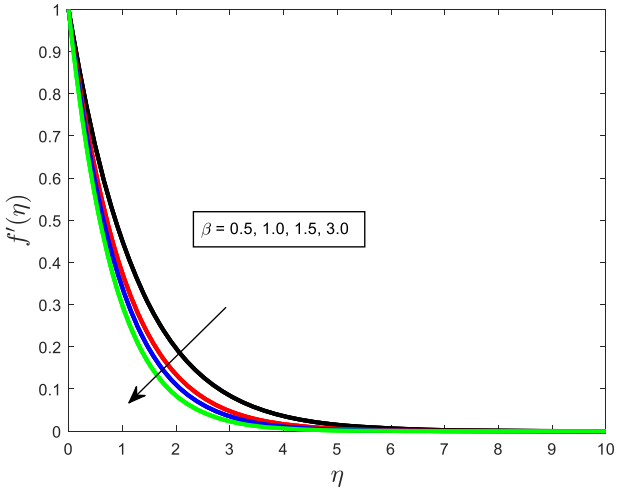


Fig. 9. Change in β on $f'(\eta)$.

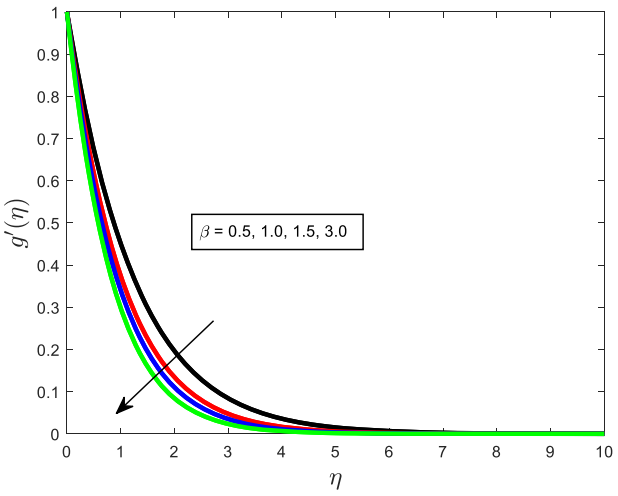


Fig. 10. Change in β on $g'(\eta)$.

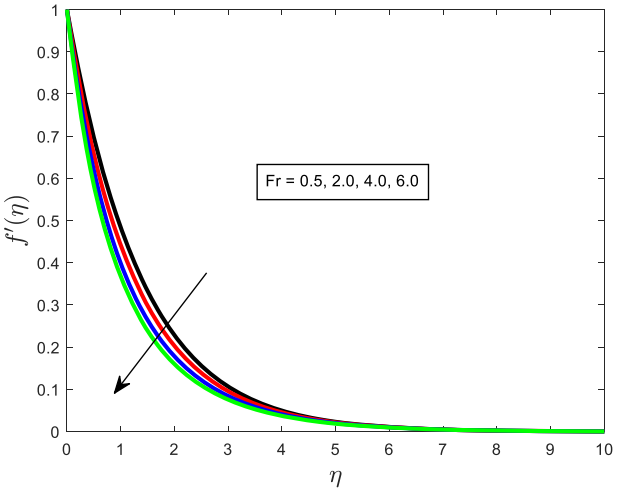


Fig. 11. Change in *Fr* on $f'(\eta)$.

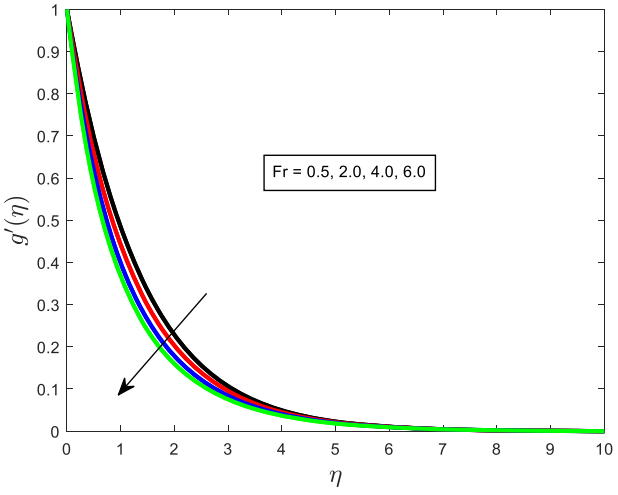


Fig. 12. Change in *Fr* on $g'(\eta)$.

thinning properties amplify flow deviations caused by external forces. Further, for the higher β the transverse velocity becomes less pronounced indicating smoother flow behavior reflecting more Newtonian response. It is because of the influence of external forces is less noticeable within the medium.

Applications: The proposed Casson fluid model is utilized to simulate blood flow through arteries, veins, etc. Variation in the Casson parameter is used to show the behavior of the blood under various shear conditions which is vital in designing medical devices like artificial heart valves, stents, etc. In daily used product like chocolate syrup, cosmetic creams the use of non-Newtonian fluid is vital.

Figs. 11, 12 exhibits the imposition of the Darcy-forchheimer inertial drag on the axial as well as transverse velocity profiles of Casson fluid. For the low values of the factor Fr, the inertial drag force became weak and the fluid velocity is predominantly influenced by the pressure gradient and the viscous effects. The axial velocity is presented its higher value with a great peak within the entire domain. With minimal resistance from the porous medium the axial velocity shows its greater impact at all points. Moreover, the increasing *Fr*, i.e. the higher *Fr*, the inertial drag starts to significantly resists the flow which leads to additional resistance from the porous matrix and the flow profile retards significantly. the resistive forces counteracts the effects of the pressure gradient and inertia making the flow slower within the flow domain leading the thinner in the bounding surface thickness. For the lower *Fr*, the inertial drag has minimal impact and the transverse velocity relatively higher and exhibits significant variations because of weak resistance. Moreover, the gradually increase in the factor *Fr*, the transverse velocity become smoother and less pronounced indicating the increased flow resistance. Therefore, for the higher *Fr*, the strong inertial drag dampens transverse velocity within the entire domain and this causes higher resistance. This lead to a thinner bounding surface and the fluid velocity retards throughout.

Applications: The Darcy-Forchheimer model is usually beneficial in optimizing the flow in porous structures i.e. filters, packed beds, etc. The increasing Fr impacts in the Casson fluid for the design of efficient filtration systems and improves the performance of industrial processes involving non-Newtonian fluids. In enhanced oil recovery where the Casson fluids are injected into porous rock formations.

The fluid temperature profile enriches for the involvment of certain factors like Eckert number, thermal radiation etc. Fig. 13 portrays the significant contribution of the Eckert number affecting the fluid temperature of the Casson fluid. The quantity *Ec* represents the ratio of the kinetic energy to the enthalpy difference in a fluid flow. Here, the conservation of the kinetic energy into thermal energy is due to viscous dissipation. Particularly, the low *Ec*, the kinetic energy contribution to thermal energy is insignificant and the temperature profile is dominated by the external thermal effects such as heat flux or the thermal boundary conditions. The viscous dissipation has least impact resulting a lower

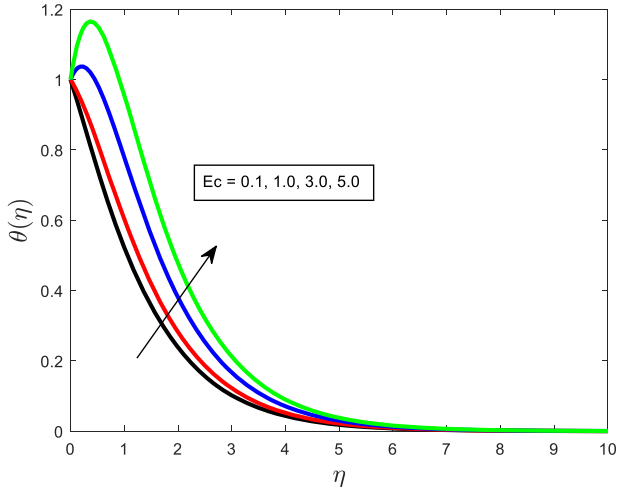


Fig. 13. Change in *Ec* on θ(η).

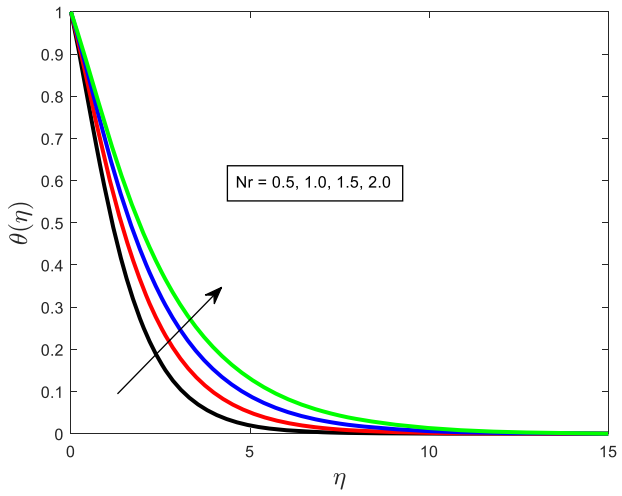


Fig. 14. Change in *Nr* on θ(η).

temperature rise within the fluid. For the higher Eckert number the viscous dissipation dominates the thermal energy contributing enhanced fluid temperature at points of the domain.

Applications: The Casson fluid are often used in industrial; systems i.e. high-speed lubrication, viscous dissipation etc. The properties of viscous dissipation show its efficient cooling mechanisms involving Casson and it also prevents thermal stability and overheating. In biomedical applications such as blood flow through artificial organs the Eckert number helps ion predicting the temperature rise due to dissipative heat.

The factor characterized by the heat flux i.e. thermal radiation and its impact on the fluid temperature distribution is depicted through Fig. 14. The quantity is a measure of the emitted wave due to the interaction of heat flux. For the low thermal radiation that records the radiative heat transfer is minimal compare to the conduction and convection. The temperature increases gradually, for the increase of thermal radiation. Further, the higher thermal radiation enhances the thermal state of fluid significantly.

Applications: The use of Casson fluid in nuclear reactor is vital due to their ability to handle high temperatures. It ensures the removal of heat from the reactor core, preventing overheating. In solar thermal systems, Casson fluids are employed in heat exchangers.

Chemical reaction plays an important role in the concentration distribution which is presented through Fig. 15. The factor is accounts for the effect of chemical reaction that takes plates within the fluid during

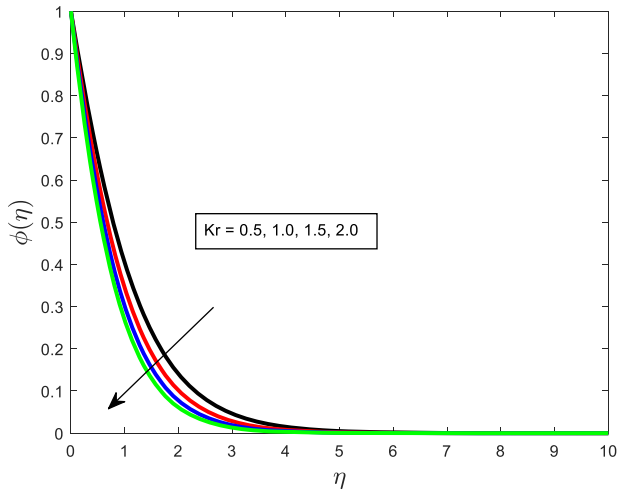


Fig. 15. Change in *Kr* on ϕ(η).

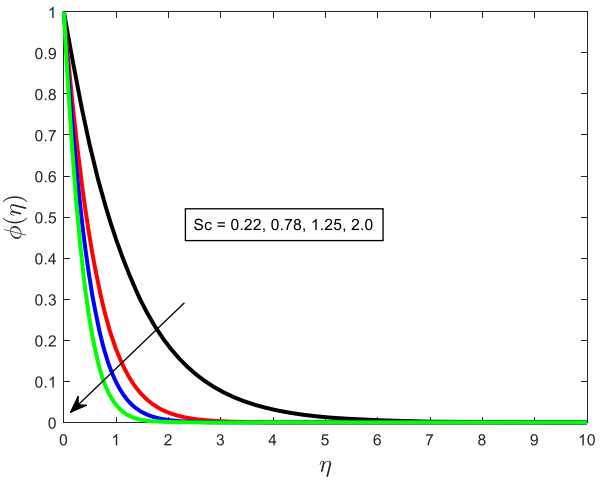


Fig. 16. Change in *Sc* on ϕ(η).

the flow. At low values of *Kr* the reaction rate is minimal and the concentration of the solute is largely unaffected by the reaction. The concentration profile is relatively uniform and the profile shows its greater impact within the flow domain. Further increasing chemical reaction the fluid concentration decreases greatly causing a thinner concentration bounding surface thickness. With the higher chemical reaction parameter, the reaction dominates the behavior of the concentration distribution.

Applications: In waste water treatment Casson fluids are often used in the process involving chemical reaction for degradation of contaminates. it impacts the rate at which the pollutants are broke down, influencing the concentration of contaminates throughout the system. Moreover, in drug delivery systems particularly when using non-Newtonian fluids, the chemical reaction parameter affects the release rate of the drug.

Fig. 16 contributes the role of Schmidt number affecting the concentration distribution of the Casson fluid. The factor *Sc* indicates the ratio of the momentum diffusivity to mass diffusivity and plays crucial role in the concentration profile of the Casson fluid. The low Schmidt number indicates the mass diffusivity is greater than that of momentum diffusivity and this causes the concentration profile become more uniform and the solute helps to spread the solute more evenly within the domain. Further, the enhanced *Sc* the concentration boundary layer is thinner which decelerates the profile throughout. In this case the momentum diffusivity dominates over mass diffusivity therefore the fluid resistance to flow is much higher than the ability of the solute diffuse. There is greater contrast between the concentration and the bulk fluid due to slower diffusion at the boundary which retards the fluid concentration.

Applications: In enhanced oil recovery processes Casson fluid are injected into oil reservoir and the Schmidt number helps in understanding the diffusion of injected chemicals within the porous medium. Moreover, in biomedical applications such as blood flow, drug delivery systems Schmidt nu8mber influences the transport of pharmaceutical agents of oxygen within the Casson fluid.

4. Conclusion

The forced convection of Casson fluid over an extending surface embedding within a porous substance is presented in this article. The energy transport phenomenon incorporates the significant characteristic of thermal radiation and the variation of the dissipative heat. Moreover, the impact of chemical reactions is investigated by inserting in the concentration distribution. The flow profile results for the contributing factors variation are obtained and presented in the discussion section. The important observations are;

- The inclusion of thermal radiation play a momentous role in enhancing the heat transport properties of the Casson fluid.
- The dissipative heat impact conducted for the involvement of the Eckert number favors in augmenting the thermal state of fluid significantly.
- The inertial drag due to the Darcy-Forchheimer model attenuates the fluid velocity in both the axial and transverse direction along with the resistivity offered by the pores substance.
- The chemical species along with the heavier species used as controlling parameter for the fluid concentration.
- The study is useful for the various applications like oil recovery processes, in biomedical systems such as drug delivery, and in environmental engineering for pollutant dispersion and water treatment processes.

Declaration of competing interest

The authors declare that they have no known competing financial interests or personal relationships that could have appeared to influence the work reported in this paper.

Data availability

No data was used for the research described in the article.

References

1. Saleem M, Al-Zubaid A, Radwan N, Saleem S, Adawi H. Thermal effects of ternary Casson nanofluid flow over a stretching sheet: an investigation of Thomson and Troian velocity slip. *Case Stud Therm Eng*. 2024;65, 105561.
2. Saleem M, Afzaal MF, Shahzadi A, Hussain M. Comparative study of Hiemenz flow in hybrid Carreau nanofluid (Fe_3O_4-Cu/kerosene-engine oil): nonlinear effects, newtonian heating and viscous dissipation. *Int J Model Simul*. 2024:1–27.
3. Saleem M, Hussain M, Ould Sidi M, Iqbal Z, Alqahtani B. Numerical examination of the Darcy–Forchheimer Casson model with instigation energy and second-order momentum slip: thermal features. *Numer Heat Transf Part B Fundam*. 2024;85(7):940–963.
4. Krishna MV, Swarnalathamma BV, Bharathi K. Thermal radiation, newtonian heating, hall and ion slip effects on unsteady MHD rotating convective flow of Casson fluid past an infinite smooth vertical porous surface. *Results Eng*. 2024;25, 103588.
5. Mustafa M, Hayat T, Pop I, Aziz A. Unsteady boundary layer flow of a Casson fluid due to an impulsively started moving flat plate. *Heat Transf Asian Res*. 2011;40(6):563–576.
6. Baithalu R, Mishra SR, Pattnaik PK, Panda S. Analysis of heat and mass transfer rates in conducting Casson fluid flow over an expanding surface considering ohmic heating and Darcy dissipation effects. *Partial Differ Equ Appl Math*. 2024;12, 100972.
7. Ul-Haq S, Ashraf MB, Tanveer A. Artificial neural network analysis of natural convection of Casson fluid flow over a curved stretching surface with viscous dissipation. *Int J Thermofluids*. 2024;24, 100973.
8. Manjunatha S, Puneeth V, Gireesha BJ, Chamkha A. Theoretical study of convective heat transfer in ternary nanofluid flowing past a stretching sheet. *J Appl Comput Mech*. 2022;8(4):1279–1286.
9. Nazir U, Sohail M, Hafeez MB, Krawczuk M. Significant production of thermal energy in partially ionized hyperbolic tangent material based on ternary hybrid nanomaterials. *Energies*. 2021;9(21):6911.
10. Wahid NS, Arifin NM. Khashi'ie NS, Pop I. Hybrid nanofluid slip flow over an exponentially stretching/shrinking permeable sheet with heat generation. *Mathematics*. 2020;9(1):30.
11. Ali A, Ahmed M, Ahmad A, Nawaz R. Enhanced heat transfer analysis of hybrid nanofluid over a Riga plate: incorporating Lorentz forces and entropy generation. *Tribol Int*. 2023;188, 108844.
12. Ali A, Das S, Jana RN. Oblique rotational dynamics of chemically reacting tri-hybridized nanofluids over a suddenly moved plate subject to hall and ion slip currents, newtonian heating and mass fluxes. *J Indian Chem Soc*. 2023;100(4), 100983.
13. Rehman S, Alfaleh A, Afef K, Shah SIA. Onset about isothermal flow of Carreau liquid over converging channel with Cattaneo-Christov heat and mass fluxes. *Heliyon*. 2023;9(5).
14. Baithalu R, Mishra SR. On the free convection of magneto-micropolar fluid in association with thermal radiation and chemical reaction and optimized heat transfer rate using response surface methodology. *Mod Phys Lett B*. 2023;37(33), 2350171.
15. Pattnaik PK, Mishra SR, Panda S. Response surface methodology on optimizing heat transfer rate for the free convection of micro-structured fluid through permeable shrinking surface. *Eur Phys J Plus*. 2024;139(3):221.
16. Hayat T, Khan MI, Khan TA, Khan MI, Ahmad S, Alsaedi A. Entropy generation in Darcy-Forchheimer bidirectional flow of water-based carbon nanotubes with convective boundary conditions. *J Mol Liq*. 2018;265:629–638.
17. Muhammad R, Khan MI, Jameel M, Khan NB. Fully developed Darcy-Forchheimer mixed convective flow over a curved surface with activation energy and entropy generation. *Comput Methods Prog Biomed*. 2020;188, 105298.
18. Almarashi AM, Algarni A, Rooman M, Shah Z, Garalleh HA. Entropy generation and heat transfer analysis of unsteady micropolar magnetized hybrid-nanofluid flow over a radially stretchable permeable rotating disk with viscous and joule dissipation effects. *Int J Thermofluids*. 2024;23, 100802.
19. Baithalu R, Mishra SR, Pattnaik PK, Panda S. Optimizing shear and couple stress analysis for the magneto-micropolar dissipative nanofluid flow toward an elongating surface: a comprehensive RSM-ANOVA investigation. *J Therm Anal Calorim*. 2023;149:1697–1713.
20. Aly EH, Rosca AV, Rosca NC, Pop I. Convective heat transfer of a hybrid nanofluid over a nonlinearly stretching surface with radiation effect. *Mathematics*. 2021;9:2220.
21. Bellman RE, Kalaba RE. Quasilinearization and nonlinear boundary-value problems. *Mod Anal Comput Methods Sci Math*. 1965;3.
22. Motsa SS. A new spectral local linearization method for nonlinear boundary layer flow problems. *J Appl Math*. 2013;2013. Article ID 423628.
23. Yanala DR, Kumar MA, Bejawada SG, Nisar KS, Raju KS, Rao VS. Exploration of heat and mass transfer on 3-D radiative MHD Casson fluid flow over a stretching permeable sheet with chemical reaction. *Case Stud Therm Eng*. 2023;51, 103527.
24. Rafiq MY, Abbas Z, Tariq A, Durrani A, Khaliq S. Viscous dissipation effects on the thermal radiatively induced micropolar fluid using the metachronal wave of cilia in the presence of slip constraints. *Adv Mech Eng*. 2024;16(12), 16878132241308930.
25. Mujahid M, Abbas Z, Rafiq MY. A study on the pressure-driven flow of magnetized non-Newtonian Casson fluid between two corrugated curved walls of an arbitrary phase difference. *Heat Transf*. 2024;53(8):4510–4527.
26. Shahzad H, Abbas Z, Rafiq MY. Molecular dynamics study of the thermal radiatively pressure-driven flow of two immiscible hybrid nanofluids through a curved pipe with viscous dissipation. *Chaos Solitons Fractals*. 2024;188, 115552.
27. Shahzad H, Abbas Z, Rafiq MY. Rheological impact of viscous fluid in the core region of heated curved pipe surrounded by Casson rheological fluid. *Case Stud Therm Eng*. 2024;61, 105156.
28. Abbas Z, Izhar Q, Rafiq MY, Ali A. Thermally oscillatory flow inside an irregular channel through a porous medium with velocity and temperature slips. *Case Stud Therm Eng*. 2024;60, 104646.
29. Bejawada SG, Yanala DR. Finite element soret dufour effects on an unsteady MHD heat and mass transfer flow past an accelerated inclined vertical plate. *Heat Transf*. 2021;50(8):8553–8578.
30. Reddy YD, Goud BS, Khan MR, Elkotb MA, Galal AM. Transport properties of a hydromagnetic radiative stagnation point flow of a nanofluid across a stretching surface. *Case Stud Therm Eng*. 2022;31, 101839.
31. Kumar MA, Reddy YD, Goud BS, Rao VS. An impact on non-Newtonian free convective MHD Casson fluid flow past a vertical porous plate in the existence of Soret, Dufour, and chemical reaction. *Int J Ambient Energy*. 2022;43(1):7410–7418.
32. Shankar Goud B, Yanala DR, Wakif A. Numerical analysis on the heat and mass transfer MHD flow characteristics of nanofluid on an inclined spinning disk with heat absorption and chemical reaction. *Heat Transf*. 2023;52(5):3615–3639.
33. Bejawada SG, Reddy YD, Jamshed W, et al. Comprehensive examination of radiative electromagnetic flowing of nanofluids with viscous dissipation effect over a vertical accelerated plate. *Sci Rep*. 2022;12(1), 20548.